Available online at www.sciencedirect.com

ScienceDirect

Advances in Space Research 69 (2022) 1130–1145

ADVANCES IN SPACE RESEARCH (a COSPAR publication)

www.elsevier.com/locate/asr

Detecting the distribution of grass aboveground biomass on a rangeland using Sentinel-2 MSI vegetation indices

C. Munyati

Department of Geography and Environmental Science, North-West University, Private Bag X2046, Mmabatho 2735, South Africa

Received 11 March 2021; received in revised form 8 October 2021; accepted 25 October 2021
Available online 29 October 2021

Abstract

Quantifying the grass biomass content of rangelands is potentially useful to rangeland managers. This study assessed the potential of image-derived vegetation indices to assess *in-situ* spatial variations in grass aboveground biomass (AGB). Sampling was conducted at the peak growth stage, at widely distributed sampling sites whose grass cover homogeneity was wider than 20 m. Up to three AGB samples per site were collected, in 1 m quadrats. Dry biomass weights were determined and averaged per site. Rainy season Sentinel-2 MSI images of the rangeland that corresponded with the fieldwork dates were obtained. Atmospheric correction of the images was performed using the Sen2Cor algorithm, which yielded 20 m resolution visible (vis), red edge (RE), near infrared (NIR), and short wave infrared (SWIR) bands. Seven biomass-sensitive vegetation indices that utilised Sentinel-2 MSI *vis-RE-NIR-SWIR* spectral ranges were then tested using the images, to determine which correlated best with the field-derived AGB. They were the Normalized Difference Vegetation Index (NDVI), Enhanced Vegetation Index (EVI), Soil Adjusted Vegetation Index (SAVI), Normalized Difference Red Edge index (NDRE), Red Edge Inflection Point (REIP), Aerosol Free Vegetation Index ($AFRI_{2.1\mu m}$), and Normalized Difference Water Index (NDWI). In decreasing order of magnitude, the EVI, SAVI, NDVI, $AFRI_{2.1\mu m}$, and NDWI had statistically significant correlations with AGB ($p \leq 0.05$). The discontinuous canopies but high biomass of tall-grass species weakened the correlations. The EVI model of AGB was then used for depicting rangeland-scale, location-context spatial variations in AGB. Pixels with woody vegetation cover $\geq 50\%$ were excluded using a binary mask that was developed through sub-pixel classification of a grass-senescence period Sentinel-2 MSI image. A statistically significant linear relationship ($F = 21.192$, $p = 0.000$) between EVI-predicted and actual AGB was established ($r = 0.765$, $p < 0.001$). The results from the studied savannah rangeland suggest higher vegetation index prediction accuracy at short-grass than tall-grass sites.
© 2021 COSPAR. Published by Elsevier B.V. All rights reserved.

Keywords: Biomass modelling; Radiometric calibration; Rangeland management; Multispectral sensors

1. Introduction

Rangelands provide vital ecosystem services, including the provision of habitats that support biodiversity conservation and the tourism industry, regulating river flows by facilitating ground water recharge, and contributing to food security through the provision of forage for livestock (Lund, 2007; Scheiter et al., 2019). Sustainability of rangeland quality requires that rangeland managers have access to timely data on the condition of the rangelands (Porter et al., 2014). In fire-prone rangelands, such as savannahs, data on the amounts and distribution of grass biomass can enable rangeland managers to plan when and where controlled fires are required, for the purpose of reducing fire fuel loads that can cause large and destructive fires (Mbow et al., 2004). Determining the grass aboveground biomass (AGB) content of savannah rangelands is, therefore, potentially beneficial for grazing management, in

E-mail address: chrismunyati@yahoo.co.uk

https://doi.org/10.1016/j.asr.2021.10.048
0273-1177/© 2021 COSPAR. Published by Elsevier B.V. All rights reserved.

both nature conservation and agricultural systems (Palmer et al., 2016).

The AGB content can be estimated using remotely sensed imagery, which has the advantage of being repetitive and non-destructive (Butterfield and Malmström, 2009; Calders et al., 2015), thereby enabling periodic monitoring of the changes. Examining the capabilities of a given sensor for use in estimating location-context spatial variations in the AGB of a grassland ecosystem is, therefore, beneficial. A number of recent studies in different rangeland types (e.g. Mundava et al., 2015; Louhaichi et al., 2018) have sought to establish protocols and techniques for non-destructive estimation of AGB using imagery.

Studies that have developed a relationship between *in-situ* AGB of grass and imagery have commonly tested the predictive accuracy of vegetation indices (e.g. Samimi and Kraus, 2004; Numata et al., 2007; Butterfield and Malmström, 2009; Duan et al., 2012; Barrachina et al., 2015; Western et al., 2015; Quan et al., 2017; Tsalyuk et al., 2017). A number of indices have been tested, commonly the Normalised Difference Vegetation Index (NDVI) in comparison with at least one other vegetation index (VI), including derivatives of the NDVI like the Soil Adjusted Vegetation Index (SAVI) and the Enhanced Vegetation Index (EVI), among others. Imagery at various spatial resolutions and from different sensors has been employed in such studies. Examples are 10 m resolution *Système Pour l'Observation de la Terre* 5 (SPOT 5) High Resolution Geometric - HRG (Chen et al., 2011b), 20 m resolution SPOT 4 High Resolution Visible Infrared - HRVIR (e.g. Dusseux et al., 2015), 30 m resolution Landsat 5/7 Thematic Mapper (TM)/Enhanced Thematic Mapper plus (ETM +) and Landsat 8 Operational Land Imager - OLI (e.g. Schino et al., 2003), as well as 250 m resolution MODerate resolution Imaging Spectrometer - MODIS (e.g. Chen et al., 2011a; Baghi and Oldeland, 2019).

The NDVI (Rouse et al., 1974), which exploits the contrast between the cellular arrangement-dependent high near infrared (NIR) reflectance and high absorption of red due to chlorophyll in non-senescent vegetation, has been found to correlate with vegetation biomass. It is computed as: $[(\rho NIR - \rho Red)/(\rho NIR + \rho Red)]$, where ρNIR and ρRed are spectral bidirectional reflectance factors at NIR and Red wavelengths, respectively. Since the NDVI is susceptible to errors introduced by variations in solar radiation and viewing geometry, soil background, and atmospheric effects, alternative indices that reduce these errors, especially in sparsely vegetated scenes, have been sought (Rondeaux et al., 1996). The SAVI minimises the effect of soil reflectance through the inclusion of a canopy background adjustment factor, L, into the NDVI denominator (Huete, 1988). Improvements on the SAVI have included the Modified SAVI (MSAVI; Qi et al., 1994) and Optimised SAVI (OSAVI; Rondeaux et al., 1996). The EVI, which was developed to optimise the vegetation signal, is a three-band (NIR, red, blue) normalised ratio index with L set to 1, and two coefficients ($C_1 = 6$, $C_2 = 7.5$) which correct for atmospheric aerosol scattering (Huete et al., 2002). Baghi and Oldeland (2019) examined the accuracy of such soil-adjusted VIs at predicting grass AGB in semi-arid environments, in comparison with the NDVI. They found that the NDVI performed best, while the SAVI and a version of the MSAVI (MSAVI2) had poorer performance. Porter et al. (2014) established that red edge bands, along with red and NIR, are responsive to pasture biomass at boot and peak growth stages, while short-wave infrared (SWIR) bands increased the predictive accuracy for the senescent stage. VIs that employ the absorption feature in the 2000 to 2200 nm region due to cellulose and lignin can detect dry plant biomass (Guerschman et al., 2009). Therefore, in addition to the NIR and red spectral regions, VIs employing the red edge and SWIR have potential for predicting AGB. Karnieli et al. (2001) devised a VI, called the Aerosol Free Vegetation Index (AFRI), which employs SWIR reflectance in place of ρRed in the NDVI equation and correlates with biomass much like the NDVI. Such a NIR and SWIR-employing normalised VI is equivalent to the Normalised Difference Water Index (Gao, 1996), which was found by Chen et al. (2011b) to have stronger correlation with grass biomass than the NDVI.

AGB analyses at the peak grass growth stage would be preferable for rangeland management applications like estimating fire fuel loads and determining the differential effects of grazing intensity. Studies of AGB in savannah rangelands commonly utilise the peak grass growth stage (e.g. Palmer et al., 2016; Tsalyuk et al., 2017; Chapungu et al., 2020; Zumo et al., 2021). Field sampling of grass for the AGB analyses is commonly through destructive sampling in quadrats of various sizes, ranging from 50 cm × 50 cm (Numata et al., 2007; Duan et al., 2012; Barrachina et al., 2015; Quan et al., 2017) to 70 cm × 70 cm (Dusseux et al., 2015) and 1 m × 1 m (Schino et al., 2003; Butterfield and Malmström, 2009; Tsalyuk et al., 2017; Chapungu et al., 2020; Zumo et al., 2021). The AGB data from the field are then used to develop predictive relationships with VI data. A common approach is to develop a linear regression model between a VI and the field-sampled AGB data, of the nature $AGB = f(VI)$, where f is a function. The best predictive model has then been used to produce a rangeland grass biomass map (e.g. Dusseux et al., 2015; Chapungu et al., 2020).

The lack of transferability of the developed models to other areas has remained a problem (Eisfelder et al., 2012). There has been little consensus on the best VIs to use, given that some work well in a given grass ecosystem and not in others (Chen et al., 2011b; Barrachina et al., 2015). However, Samimi and Kraus (2004) showed that such models can be transferrable, at least to other savannah areas. Grazing pressure is a key determinant of grass biomass in these savannah rangelands (Western et al., 2015). Therefore, establishing a VI that predicts *in-situ* AGB of grass and reproduces spatial variations that are

related to the location context on the rangeland, such as grazing pressure, is useful. Duan et al. (2012) investigated this, and established a VI that best correlated with AGB for alpine grassland. In this study, the comparative accuracy of common biomass-sensitive vegetation indices that utilise visible, red edge, NIR and SWIR spectral regions at predicting grass AGB of a savannah rangeland is examined. The aim was to establish a vegetation index that best predicts the savannah rangeland's *in-situ* aboveground grass biomass by being sensitive to location context spatial variations. The specific objectives were: (1) to determine a vegetation index that reproduces field differences in aboveground biomass due to grazer utilisation, and (2) to establish the potential utility of the vegetation index for grass biomass-related rangeland management. Therefore, the study examined the usefulness of vegetation indices at the local, rangeland management scale as opposed to the regional scale.

2. Material and methods

2.1. Study area

The study area was Mafikeng Game Reserve (MGR). MGR is located on the outskirts of Mahikeng (previously called Mafikeng), the capital of the North West Province of South Africa. Fig. 1 shows the location context of MGR. It is bordered by two busy highways to the south and north. To the west is the Mahikeng Central Business District (CBD). On its eastern border are livestock and wildlife ranches.

MGR is fenced and protected as a biodiversity conservation area. It is managed by the North West Parks Board (NWPB). Its 4 800 ha have a history of a mixture of arable and livestock ranch farming. In 1992, the previously separate farmsteads were amalgamated to form the game reserve. Only wild grazer species utilise MGR. They roam freely within the confines of the fence, in a continuous (year-long) grazing system. At the time of the study, the most numerous ungulate grazer species included zebra (*Equus burchelli*), buffalo (*Syncerus caffer caffer*), impala (*Aepyceros melampus melampus*), blesbok (*Damaliscus dorcas phillipsi*), black wildebeest (*Connochaetes gnou*), warthog (*Phacochoerus africanus*), springbok (*Antidorcas marsupialis*), and red hartebeest (*Alcelaphus buselaphus caama*). The NWPB authorities manage the animal species composition inside MGR, through species introductions and relocations. The reserve's fence prevents the entry of livestock and wild-species grazers from outside.

The river in the northern sector of MGR (Fig. 1b) contains water for only a very limited period (less than two months per year). Therefore, there are acute shortages of drinking water for the animals. As a consequence, water is supplied at artificial watering points (water holes). At the time of this study, the water holes consisted of two river earth dams (WH2, WH3; Fig. 1b), and four boreholes

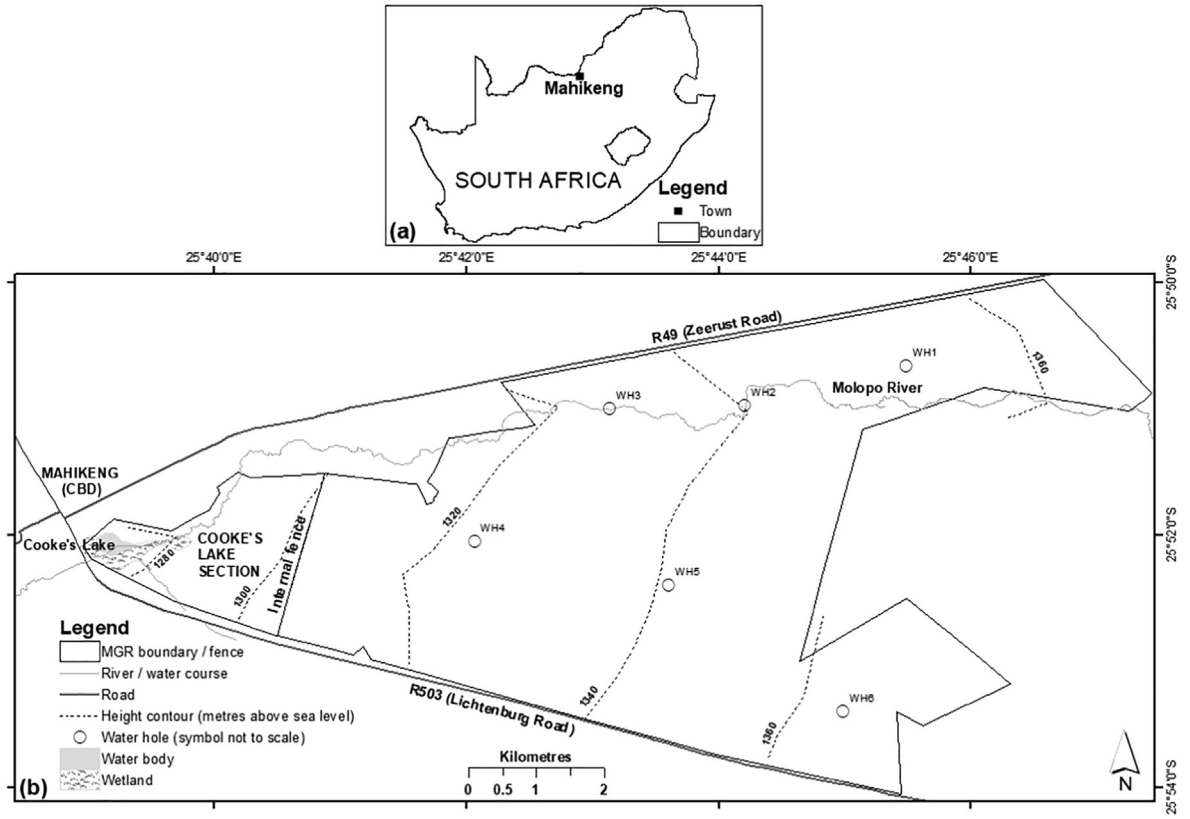

Fig. 1. Location of the study area, Mafikeng Game Reserve (MGR), in South Africa (a), and (b) its location context and physical characteristics.

away from the river valley (WH1, WH4, WH5, WH6; Fig. 1b). Being a non-equilibrium rangeland, grass biomass and rangeland quality in MGR are influenced mainly by rainfall and the water holes. Most of the rainfall is received during the rainy season between October in one year and April in the next (with a peak in January-February; Fig. 2a). The total annual rainfall is variable (Fig. 2b). The water holes cause piospheres, in which the rangeland is degraded and has little grass (Hess et al., 2020).

The common grass species in the study area are summarised in Table 1. The highest density of woody vegetation is in the river valley. Away from the valley, woody vegetation is quite sparse and grass dominant. Dry season wild fires, which can damage the woody vegetation, can potentially occur annually in the savannahs of the study area (Mucina and Rutherford, 2006). The fires can be both human and naturally-induced (e.g. by lightning or extreme heat).

At the time of the study, the grazers in MGR avoided the sections that border the two highways, tending to utilise the central region encompassed by the water holes. Therefore, the highest grazing pressure (i.e., highest grazing intensity) was in the zone encompassed by the water holes and up to the eastern fence (Fig. 1b). An artificial water body (Cooke's Lake; Fig. 1b), that was created by an earth dam across the river, sustained a wetland in the western section of MGR close to the CBD. Its hydrophyte wetland vegetation consisted mainly of reeds. An internal fence (Fig. 1b) excluded the grazers from this Cooke's Lake Section of MGR. The entry of wild fires into MGR is

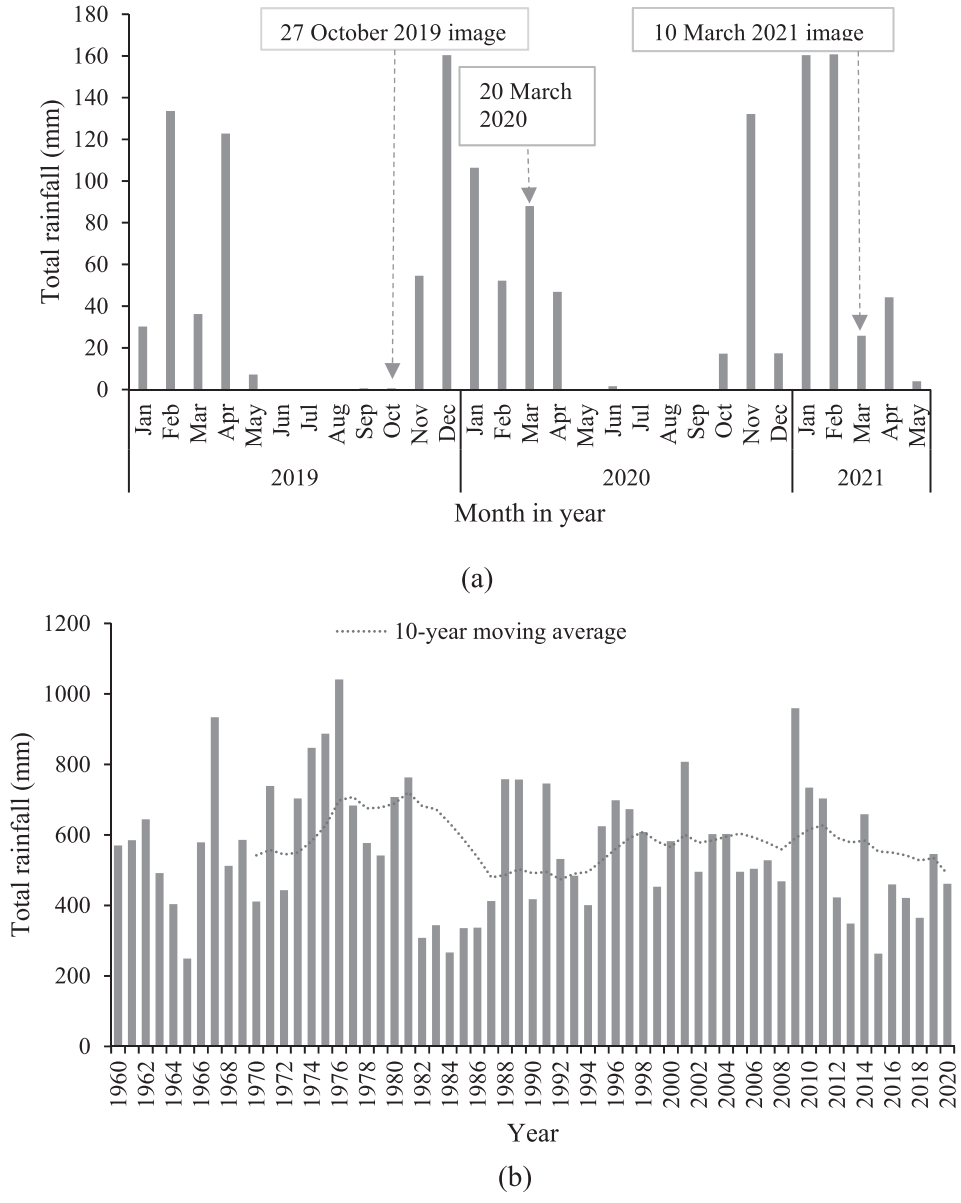

Fig. 2. Rainfall patterns for the studied rangeland as depicted by data from Mahikeng, the nearest weather station: (a) monthly rainfall in the period leading up to the image dates (dates as justified in Section 2.3), and (b) long-term rainfall. Data: South African Weather Service.

Table 1
Common grass species in the studied rangeland*.

Genus	Species	Physical form	Palatability and grazer preference
Aristida	*A. congesta* *A. meridionalis* *A. mollissima* subsp. *argentea* *A. stipitata* subsp. *stipitata*	Short grass	Most species palatable and utilised by grazers; *Aristida Congesta* is unpalatable.
Brachiaria	*B. nigropedata* *B. serrata*	Short grass	Highly palatable, high nutrition value, highly preferred by grazers.
Digitaria	*D. eriantha* subsp. *eriantha* *D. argyrograpta*	Short grass	Highly palatable, very high nutrition value, highly preferred by grazers.
Eragrostis	*E. lehmanniana* *E. pallens* *E. superba* *E. trichophora*	Short, bunch grass	Palatable, utilised by grazers. Of average nutrition value.
Heteropogon	*H. contortus*	Short, tussock grass	Palatable when young, less utilised when fully grown.
Themeda	*T. triandra*	Tall, tuft grass	Palatable, especially when young; less utilised when fully grown.
Hyparrhenia	*H. diplandra* *H. rufa*	Tall, tuft grass	Palatable when young, less utilised when fully grown.

* Compiled from literature sources (Grunow, 1980; O'Connor, 1992; Mucina and Rutherford, 2006).

restricted by perimeter fire breaks. Despite the restriction, unwanted fires occasionally do enter from outside. Therefore, the sections of MGR near the perimeter fence have higher susceptibility to unwanted fires (i.e., have higher fire incidence) than the central parts. Intentional, controlled fire is occasionally used by MGR management to reduce the accumulation of biomass that can fuel large fires in the future.

2.2. Field sampling

2.2.1. Aboveground grass biomass

AGB data were collected at the peak grass biomass stage, at the end of the grass growth season when the grass was at full maturity. Two field campaigns were used: 25–26 March 2020 (20 sampling sites; 3 in the no-grazing Cooke's Lake Section, 17 in the Main Reserve section) and 13–14 July 2021 (20 sampling sites, all in the no-grazing Cooke's Lake Section). Completing the sampling within a short time period was vital, in order to avoid changes in biomass due to phenology (Butterfield and Malmström, 2009), grazing pressure (Samimi and Kraus, 2004), or unanticipated fires. This restricted the duration of sampling during each campaign.

The sampling approach was to spread the sampling sites widely across the rangeland, through judgemental sampling. This was in order to represent grass in the different location contexts related to grazing intensity and fire incidence. The ideal grass sampling sites needed to be large enough to constitute at least a 20 m pixel, and to have uniformity in grass cover (illustrated by the sites in Fig. 3). Similar studies have also used grass cover uniformity to select AGB sampling sites (e.g. Chen et al., 2011b; Barrachina et al., 2015). The respective sampling sites fitted into one of four location context treatments (Fig. 4a): (a) high grazing intensity, low fire incidence (HGLF, sample size (n) = 9), (b) high grazing intensity, high fire incidence (HGHF, $n = 5$), (c) low grazing intensity, high fire incidence (LGHF, $n = 3$), (d) low grazing intensity, low fire incidence (LGLF, $n = 23$).

At each sampling site, a 1 m × 1 m quadrat was tossed randomly in a 20 m × 20 m plot, up to three times in low grass cover sites (an average AGB value was then used). Smaller quadrat sizes were judged to be unsuitable due to the low grass biomass in high grazing intensity sites. The low biomass would have yielded weights that could not be differentiated by the balance that was subsequently used for weighing the AGB samples. Baghi and Oldeland (2019) employed a similar approach involving three random coordinates in a plot, at which a quadrat was placed, while Schino et al. (2003) used 3–5 random quadrat samples per 1 ha plot. After each random quadrat toss, the grass inside the quadrat was collected by cutting it to the soil level. The collected grass samples were packed and labelled on site, and the Universal Transverse Mercator (UTM) coordinates of the centre of the 20 m × 20 m plot were recorded using a ± 3 m accuracy Garmin Legends® Global Positioning System (GPS). The general nature of the grasses was noted at each site.

During the 2020 sampling, the grass was still green. Therefore, the March 2020 samples were air-dried in the laboratory for a week. The July 2021 samples were already dry when collected in the field. In the laboratory, the weight of each sample was determined using a 0.1 g precision balance. The balance was not usable in the field since it required a mains power connection. Consequently the wet biomass weights, which would have enabled the determination of water content, were not determined since the samples wilted in transit to the laboratory.

2.2.2. Woody cover

When viewed perpendicularly from a vertical perspective (which is the perspective on a satellite image), the canopies of savannah trees tend to be circular (Price et al.,

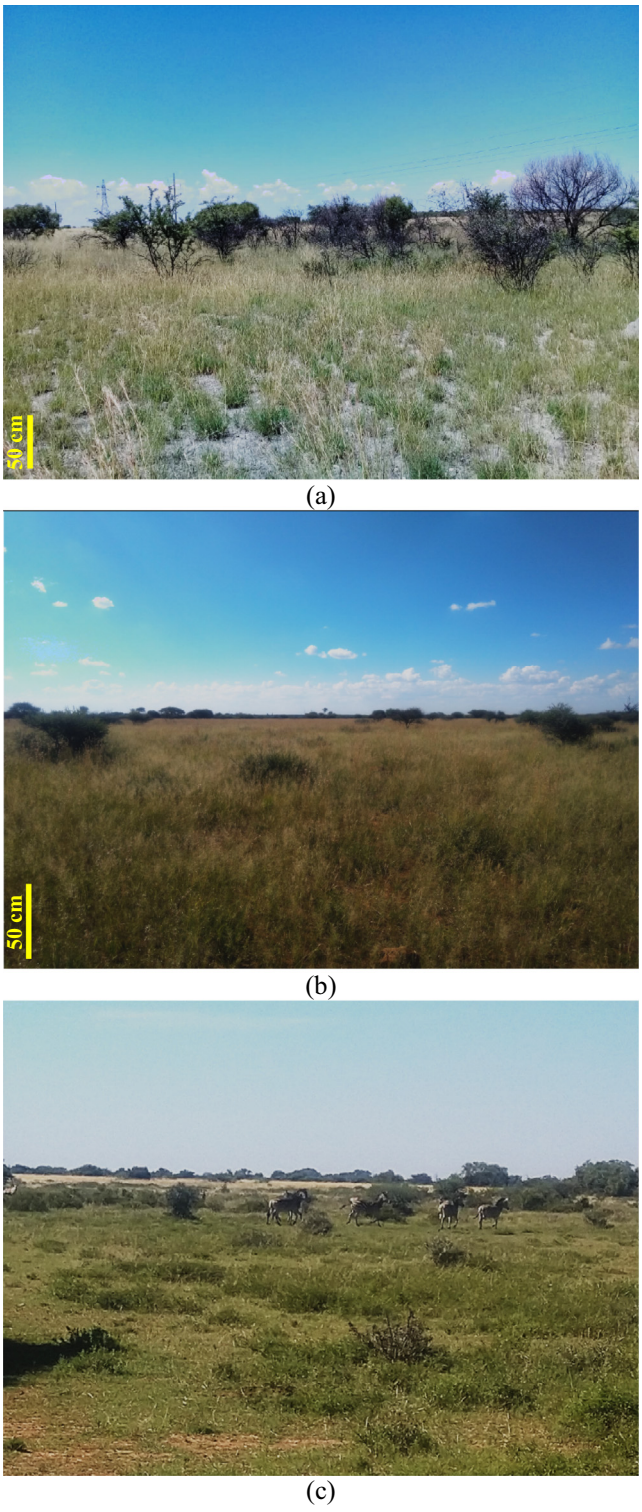

Fig. 3. Field photos (taken in March 2020) illustrating *in-situ* grass biomass and species characteristics: (a) *Hyparrhenia rufa* (foreground) with scattered (predominantly *Vachellia* (previously called *Acacia*)) woody species, (b) *Eragrostis lehmanniana* dominated grass (with *Hyparrhenia* spp.) in a lightly-grazed section, and (c) short-cropped grass in the heavily grazed south eastern sector (with zebras in the middle background). Grass flowers gave the canopy of the green grass some brown and yellow/orange tones. (For interpretation of the references to colour in this figure legend, the reader is referred to the web version of this article.)

2009). The area under woody (tree, shrub) canopies was, therefore, determined at sampling sites using an approach that estimated it based on the circular canopy model. The basis for the approach was the use of crown diameter as a predictive variable in allometric models, which assumes a circular canopy and has been shown to improve the models (Jucker et al., 2017). The goal was to obtain image classification training data on pixel woody cover fractions, and for verifying the subsequent woody cover classification. This more time-demanding sampling was conducted in April 2018 and 2019. During the sampling, canopy diameter (d) measurements of woody individuals were taken. The diameters were determined by spreading a 50 m measuring tape from the perceived starting point to the ending point of the canopy, using the view point of an orthogonal projection of the canopy to the ground. The measuring tape was spread either below or above the canopy, depending on the woody individual's height. The canopy diameter was used to determine the radius, r (as $r = \frac{1}{2}d$), and then the canopy area was computed as: $Area = \pi r^2$. The woody canopy cover was quantified in 20 m × 20 m (=400 m^2) sampling plots. The UTM coordinates of the centre of each plot were recorded using a GPS. The total canopy area per plot was then used to determine the woody cover fraction, as a percentage of the 400 m^2 area of the plot. Fourteen sampling plots were used (Fig. 4b).

2.3. Image data

Sentinel-2 MSI (Multi-Spectral Imager) imagery was selected for use due to enhanced spectral sensitivity that includes the red edge region, compared to equivalent multispectral sensors. The Sentinel-2 MSI acquires data in thirteen bands, including three red edge bands, at the spatial resolutions of 10 m, 20 m, and 60 m (Table 2). Two cloud-free, rainy season images of the rangeland acquired on 20 March 2020 (Fig. 4a) and 10 March 2021 were obtained for the analysis of grass AGB. The image dates were selected in relation to the field campaigns. The grass was already dry during the 2021 campaign. Since sampling was conducted in the no-grazing section of the rangeland, the grass biomass was still intact. The closest peak growth stage date on which a cloud-free image was available on the Sentinels image catalogue was 10 March 2021.

A cloud-free, dry season Sentinel-2 MSI image acquired on 27 October 2019 (Fig. 4b) was obtained. This image was used for eliminating pixels with woody cover (see Section 2.4.2). Due to the rainfall-dependent phenology of herbaceous vegetation, the grass was dry (except on the wetland) but the woody vegetation was in leaf on that date (there was very little rainfall prior to the date; Fig. 2a). The dates of the woody cover sampling campaigns and the dry season image were up to one and a half years apart. However, since the woody vegetation in the study area grows quite slowly (Mucina and Rutherford, 2006), the image

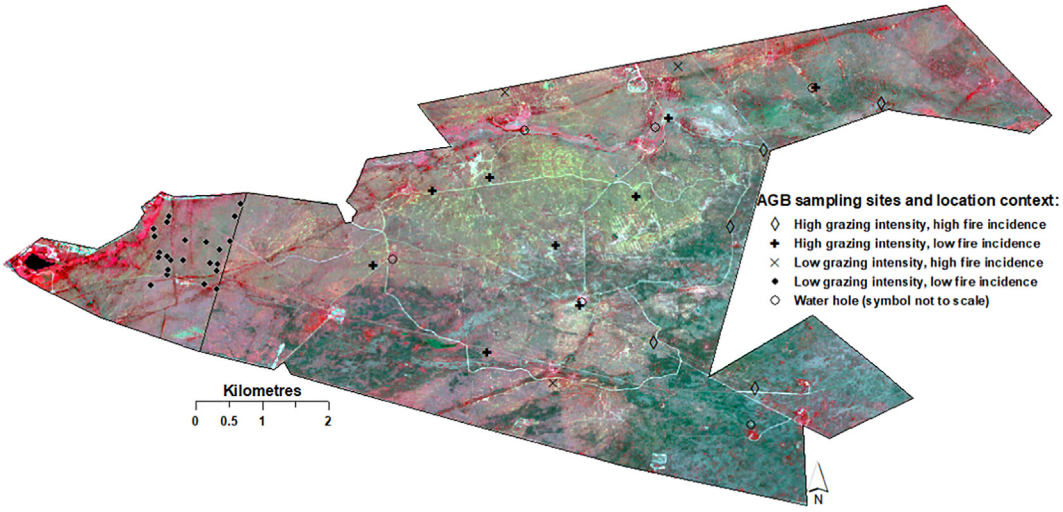

(a)

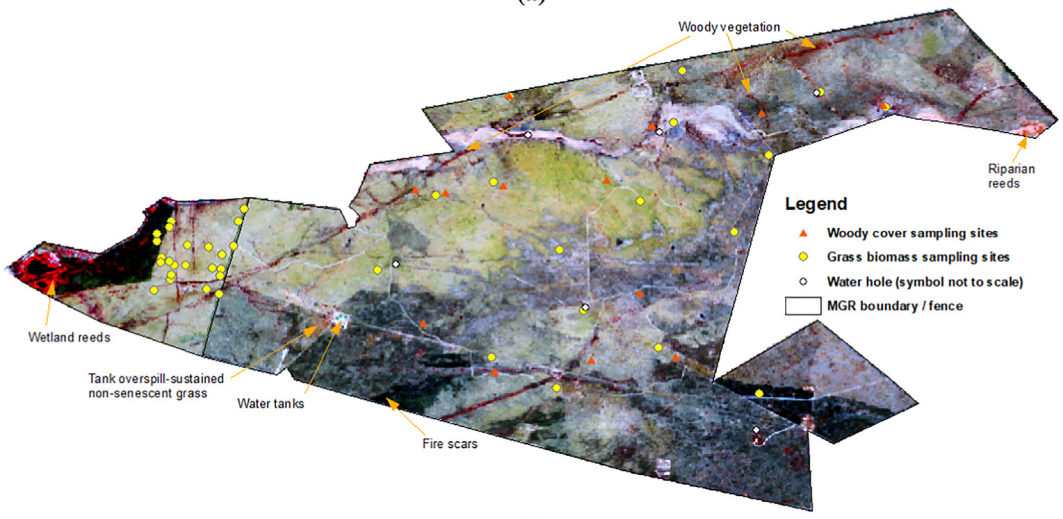

(b)

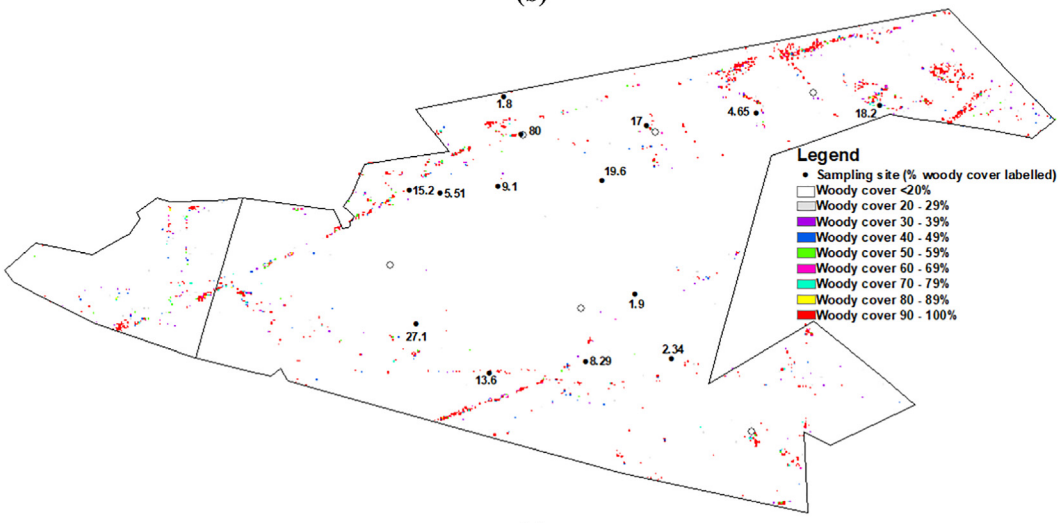

(c)

Fig. 4. Illustration of the distribution of the grass aboveground biomass (AGB) and woody cover sampling in the study area in relation to image characteristics: (a) the atmospherically-corrected 20 March 2020 (rainy season) Sentinel-2 MSI image (R,G,B = 8a,4,3) at 20 m resolution, with the AGB sampling sites indicated, (b) the atmospherically-corrected 27 October 2019 (dry season; spring) Sentinel-2 MSI image (R,G,B = 8a,4,3) at 20 m resolution, with the AGB and woody sampling sites, and (c) the woody cover in 20 m pixels as extracted from the image in (b), with the field-determined woody cover percentages labelled at the respective sampling sites. Grass was senescent on the dry season date, but the woody vegetation was in leaf on both dates. Sampling site symbols are not to scale (are magnified for visibility).

Table 2
Characteristics of the Sentinel 2 MSI bands.

Band	Spectral wavelengths (nm)			Spatial resolution (m)
	Central wavelength	Band width	Spectral range	
1 (coastal aerosol)	443	20	433–463	60
2 (blue)	490	65	458–523	10
3 (green peak)	560	35	543–578	10
4 (red)	665	30	650–680	10
5 (red edge)	705	15	698–713	20
6 (red edge)	740	15	733–748	20
7 (red edge)	783	20	773–793	20
8 (NIR)	842	115	785–900	10
8a (narrow NIR)	865	20	855–875	20
9 (water vapour)	945	20	935–955	60
10 (SWIR cirrus)	1375	30	1360–1390	60
11 (SWIR)	1610	90	1565–1655	20
12 (SWIR)	2190	180	2100–2280	20

was satisfactory despite the date differences. Fire and elephants are the main destructive agents for living savannah trees (Mucina and Rutherford, 2006). There were no elephants in MGR at the time of the study, and the occurrence of fire was restricted by MGR management. Therefore, the differences in woody canopy sizes and total woody cover between the dates were minimal.

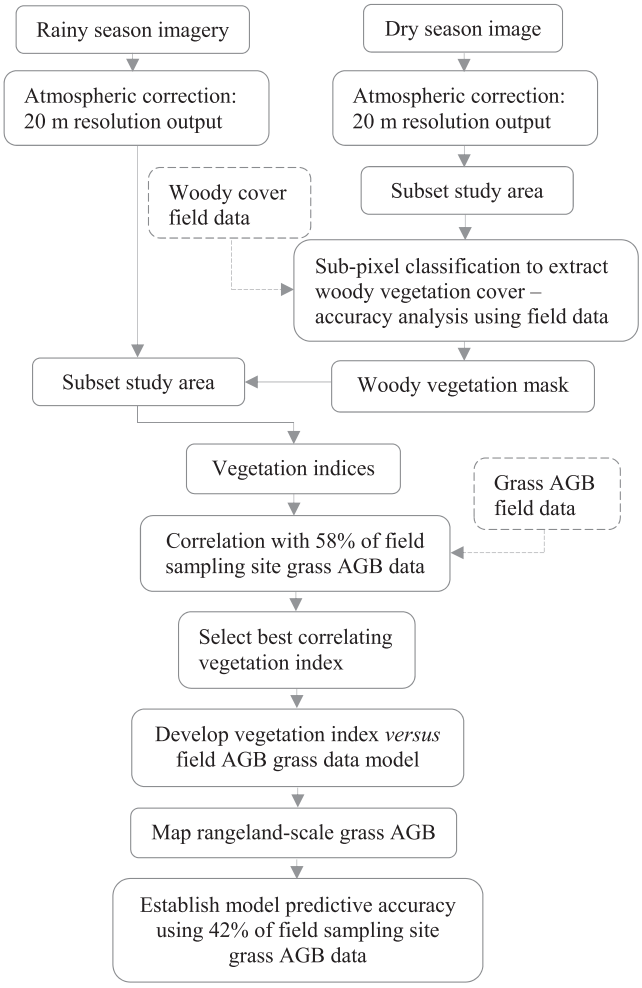

Fig. 5. Image processing flow chart.

2.4. Image processing

Fig. 5 summarises the image processing flow chain. All the image processing was performed using ERDAS Imagine 2020®.

2.4.1. Pre-processing

The Sentinel-2 MSI images were at pre-processing level 1C: as unsigned 16-bit, top-of-atmosphere (TOA) reflectance and in the UTM projection (UTM Zone 35S; WGS84 datum). Correction of the images for atmospheric effects, to obtain bottom-of-atmosphere (BOA) reflectance, was performed using the Sen2Cor® algorithm, Version 2.5.5. The algorithm is provided by the Sentinel Toolbox. It applies an operational atmospheric correction to the MSI spectral bands to retrieve atmospheric parameters from the image itself, with cirrus correction using band 10 (1 375 nm), water vapour retrieval using bands 8a and 9 (865, 945 nm) and aerosol optical depth retrieval (Martins et al., 2017). Its output is BOA reflectance images at the spatial resolutions of 10 m (bands 2, 3, 4, 8), 20 m (bands 2–7, 8a, 11, 12), and 60 m (bands 1–7, 8a, 9, 11, 12). The 10 m resolution output was not used since the red edge and SWIR bands, which were needed for some of the tested VIs, were not yielded at this resolution. Therefore, the 20 m resolution output was used since the preference was high spatial resolution while, at the same time, retaining representation of visible, red edge, NIR and SWIR reflectance. The study area was then subset from each image.

2.4.2. Masking out woody vegetation

Since the goal was to examine the grass AGB, the contribution of woody vegetation (i.e. trees, shrubs) to the reflectance values in the 20 m pixels needed to be minimised. This was accomplished by extracting woody cover on the dry season image (Fig. 4b), and then using the extracted woody cover as a mask on the rainy season image (Fig. 4a). The masked rainy season image was then used for analysing grass AGB. Extracting the woody cover was

accomplished by sub-pixel classification, which classifies objects that are smaller than the spatial resolution of the sensor (Myint, 2006).

Pure woody canopy end-members are rare for the vegetation in the study area, since canopy closure rarely reaches 100%. Therefore, the multispectral reflectance at the 20 m × 20 m field sampling plot where near-complete (80%) canopy closure was observed was specified as woody end-member signature. The signature was generated manually using the plot's pixel and the nearest neighbouring pixels. The remainder of the field sampling sites ($n = 13$) were used for classification accuracy assessment. Using the end-member spectral signature, the image was then classified into eight woody cover fractions (the highest possible in the software). The cover fractions were in increments of 10%, the lowest of which was 20–29% (i.e., 0.20–0.29, 0.30–0.39, …, 0.90–1.00). Pixels without woody vegetation or whose woody cover was <20% were left unclassified.

A woody vegetation image mask was then created from the classified woody cover fraction image. Pixels whose woody cover was at least 50% were considered as not ideal for the quantification of grass AGB. Therefore, all woody cover fractions above 49% were re-coded as zero, and the cover fractions in the range 0–49% as one. The resulting re-coded, 20 m resolution thematic image was then multiplied by each of the 20 m resolution bands of the 2020 rainy season image, which gave the high woody cover pixels a digital number (DN) of zero. The composite image resulting from this, with high woody content pixels masked out, was then used for mapping the rangeland-scale distribution of grass AGB using the optimal AGB-VI function.

2.4.3. Vegetation indices

Seven biomass-sensitive vegetation indices that utilise spectral regions in which the Sentinel-2 MSI sensed were tested for their accuracy at detecting spatial variations in the AGB field data. The indices were the NDVI, SAVI, EVI, NDWI, $AFRI_{2.1\mu m}$, Normalised Difference Red Edge Index (NDRE), and Red Edge Inflection point (REIP). Their respective equations are as in Table 3. The output of the REIP equation is the wavelength (λ) of the red edge inflection point, in nanometres (nm). To generate pixel values of the respective vegetation indices, the Sen2Cor-produced BOA reflectance (with woody cover masked out as in Section 2.4.2) in visible, red edge, NIR and SWIR bands at the same spatial resolution (20 m) was used as image data input. The respective index equations were implemented by assembling model flows that used the respective bands, using the Model Maker function in ERDAS Imagine 2020®.

2.5. Statistical analysis

The strength of the relationship between each VI in Table 3 and the field-determined grass AGB data was tested using Pearson's product moment correlation coefficient (r) values. This analysis used the AGB data from

Table 3
List of the biomass-sensitive vegetation indices tested.

Vegetation index	Equation (where ρ = reflectance; B = band; $L = 0.5$)		Reference
	General	Applied to Sentinel-2 MSI bands	
Normalised Difference Vegetation Index (NDVI)	$NDVI = \left(\frac{\rho NIR-\rho Red}{\rho NIR+\rho Red}\right)$	$NDVI = \left(\frac{\rho B8a_{865nm}-\rho B4_{665nm}}{\rho B8a_{865nm}+\rho B4_{665nm}}\right)$	Rouse et al. (1974)
Soil Adjusted Vegetation Index (SAVI)	$SAVI = \left(\frac{\rho NIR-\rho Red}{\rho NIR+\rho Red+L}\right)\times(1+L)$	$SAVI = \left(\frac{\rho B8a_{865nm}-\rho B4_{665nm}}{\rho B8a_{865nm}+\rho B4_{665nm}+L}\right)\times(1+L)$	Huete (1988)
Enhanced Vegetation Index (EVI)	$EVI = 2.5\left(\frac{\rho NIR-\rho Red}{\rho NIR+6\rho Red-7.5\rho Blue+1}\right)$	$EVI = 2.5\left(\frac{B8a_{865nm}-\rho B4_{665nm}}{\rho B8a_{865nm}+6\rho B4_{665nm}-7.5\rho B2_{490nm}+1}\right)$	Huete et al. (2002)
Normalised Difference Red Edge index (NDRE)	$NDRE = \frac{\rho 780-\rho 730}{\rho 780+\rho 730}$	$NDRE = \frac{\rho B7_{783nm}-\rho B6_{740nm}}{\rho B7_{783nm}+\rho B6_{740nm}}$	Peng and Gitelson (2012)
Normalised Difference Water Index (NDWI)	$NDWI = \left(\frac{\rho 0.86\mu m-\rho 1.24\mu m}{\rho 0.86\mu m+\rho 1.24\mu m}\right)$	$NDWI = \left(\frac{\rho B8a_{865nm}-\rho B11_{1610nm}}{\rho B8a_{865nm}+\rho B11_{1610nm}}\right)$	Gao (1996)
Aerosol Free Vegetation Index (AFRI)	$AFRI_{2.1\mu m} = \left(\frac{\rho NIR-0.5\rho SWIR_{2.1\mu m}}{\rho NIR+0.5\rho SWIR_{2.1\mu m}}\right)$	$AFRI_{2.1\mu m} = \left(\frac{\rho B8a_{865nm}-0.5\rho B12_{2190nm}}{\rho B8a_{865nm}+0.5\rho B12_{2190nm}}\right)$	Karnieli et al. (2001)
Red Edge Inflection Point (REIP)	$REIP = 700+40\left(\frac{\frac{(\rho 670+\rho 780)}{2}-\rho 700}{\rho 740-\rho 700}\right)$	$REIP = 700+40\left(\frac{\frac{(\rho B4_{665nm}+\rho B7_{783nm})}{2}-\rho B5_{705nm}}{\rho B6_{740nm}-\rho B5_{705nm}}\right)$	Clevers et al. (2002)

the 23 sites (i.e. 58% of the field sampling sites) in the no-grazing section of the rangeland, whose data were collected during the 2021 field campaign. The respective VI values at these sites were obtained using the 10 March 2021 image.

Equations that related the AGB values to their corresponding index values were then developed for the seven VIs tested. Linear, logarithmic, polynomial, and power functions were tested. The function (model) that yielded the highest coefficient of determination (R^2) value was selected as the optimal model. The AGB data from the 2020 field campaign ($n = 17$ sites, 42% of the sampling sites) were used for model validation. Their respective VI values were obtained using the 20 March 2020 image. A relationship with which to predict rangeland AGB values was then developed by linear regression of the validation site AGB values on their model-predicted values.

2.6. Rangeland-scale depiction of grass AGB

The optimal VI model (i.e. with the highest coefficient of determination (R^2) value; Section 2.5) was selected for predicting AGB values on the rangeland. The model was then applied on the reflectance data that were contained on the woody cover-masked 2020 image. Rangeland-scale spatial variations in grass AGB were then depicted. Due to the limited sample size, eliminating AGB data with large residuals (i.e. model refinement) was not performed.

3. Results

3.1. Grass biomass

The grass AGB ranged between 95.2 g m^{-2} (i.e. 952 kg ha^{-1}) on the short grass at high grazing intensity sites, and 1 005 g m^{-2} (i.e. 10 050 kg ha^{-1}) at sites with tall grass species. Therefore, sites that were dominated by tall grass species tended to have high AGB values but discontinuous canopies. Excluding such sites (since tall grass species were avoided by the grazers) showed that the mean AGB values per treatment from the 2020 sampling sites were in the order HGHF ($\bar{x} = 189.9$ g m^{-2}), HGLF ($\bar{x} = 216.1$ g m^{-2}), LGLF ($\bar{x} = 219.7$ g m^{-2}), and LGHF ($\bar{x} = 328.5$ g m^{-2}). There was a statistically significant difference between the AGB means of the HGHF and LGHF treatments ($t = 2.772$; $p = 0.05$). Therefore, high grazing intensity had more influence on AGB than fire frequency.

3.2. Woody cover

The woody cover fractions at the field sampling sites are shown in Fig. 4c. Eleven of the 13 field sampling sites (i.e., excluding the site that was used for spectral signature development) were assigned to their correct woody cover fractions, giving a classification accuracy of 85%. Overall, the rangeland had very little woody cover and was dominated by expanses of grass (illustrated by the field photos in Fig. 3).

3.3. Correlation of grass AGB with vegetation indices

Five of the seven VIs yielded statistically significant correlations with grass AGB (Table 4). In decreasing order of correlation coefficient values, the VIs were the EVI, SAVI, NDVI, $AFRI_{2.1\mu m}$, and NDWI. Therefore, the red edge VIs had lower AGB predictive accuracy, both of which yielding non-significant correlations ($p > 0.05$). The SAVI performed only marginally better than the NDVI.

The predictive models of the five VIs with statistically significant correlations (Fig. 6) were all potentially suitable for predicting rangeland scale-grass AGB. However, the EVI's model was utilised for mapping the rangeland-scale distribution of grass AGB since it had the highest coefficient of determination ($R^2 = 0.2534$). For comparison, the next best correlating VI's model (the SAVI) was also applied. The resulting rangeland-scale distributions are shown in Fig. 7.

3.4. Vegetation index-modelled grass biomass in location context

The correlation between the EVI-predicted and actual AGB values from the validation sites (Fig. 8) was statistically significant ($r = 0.765$, $p < 0.001$). Linear regression of the actual AGB values on the EVI-predicted values yielded a statistically significant slope ($F = 21.192$, $p = 0.000$).

The EVI-modelled grass AGB (Fig. 7b) correctly depicts low biomass in the highly grazed central-eastern sections of the study site, in comparison with the no-grazing western and lightly grazed south-western sections. The highly grazed zone, encompassed by the water holes, had high grazer utilisation due to proximity to the water sources. Sections of the rangeland that are close to the southern and northern fences are also correctly depicted as having slightly higher biomass, due to lower grazer utilisation frequency.

From the EVI model, the majority of the 20 m pixels had grass AGB in the range 388.8–494.9 g m^{-2} (mode = 449.8 g m^{-2}), as shown in Fig. 9. Based on the fre-

Table 4
Correlation coefficient values between sample site aboveground biomass and vegetation indices.

Vegetation index	Correlation coefficient (r)	Probability (p) and significance
EVI	0.426	$p < 0.05$*
SAVI	0.419	$p < 0.05$*
NDVI	0.417	$p < 0.05$*
$AFRI_{2.1\mu m}$	0.414	$p < 0.05$*
NDWI	0.412	$p \approx 0.05$*
REIP	0.366	$p > 0.05$, NS
NDRE	0.268	$p > 0.05$, NS

* = significant at 5%, NS = not significant.

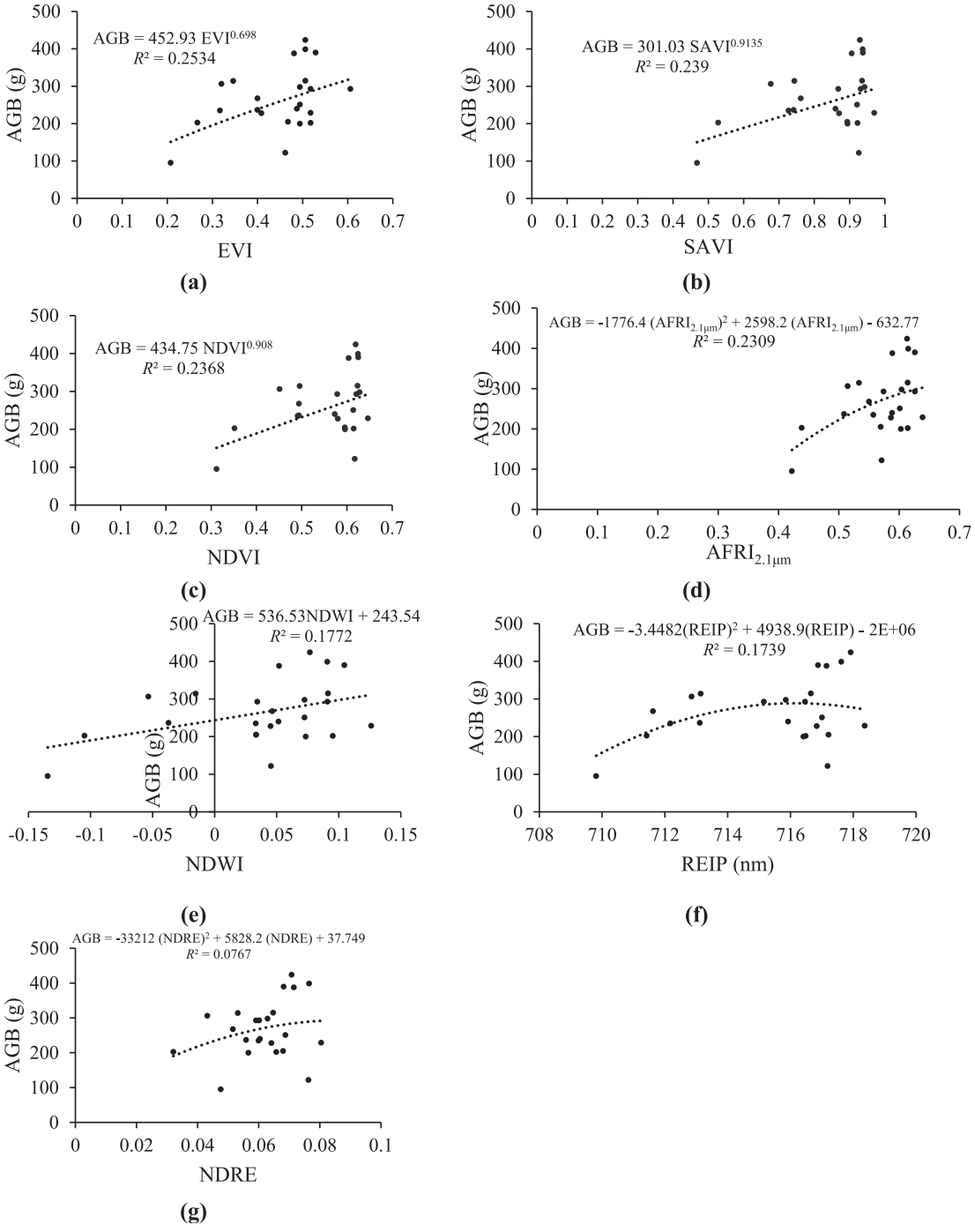

Fig. 6. Scatter plots and best-fit functions showing the relationship between sampling site grass aboveground biomass (AGB) and vegetation index values for the indices in Table 3.

quency distribution of grass biomass per pixel in Fig. 9, the rangeland had approximately 20 444.7 tons of dry herbaceous biomass on the image date.

4. Discussion

4.1. Grass biomass

The AGB values from the study area that were derived in this study were low, in comparison with similar rangelands. From sampling sites in Madikwe Game Reserve, which is located about 100 km northeast of the study area, Samimi and Kraus (2004) determined grass AGB values ranging between 2 750 kg ha^{-1} and 6 980 kg ha^{-1}. The results that were derived in this study showed that MGR had grass AGB in the range 95.2 g m^{-2} (i.e. 952 kg ha^{-1}) to 1 005 g m^{-2} (i.e. 10 050 kg ha^{-1}).

The possible cause of the lower biomass is that grazing intensity was higher in MGR. The positive skew in the frequency distribution of the biomass values in Fig. 9 indi-

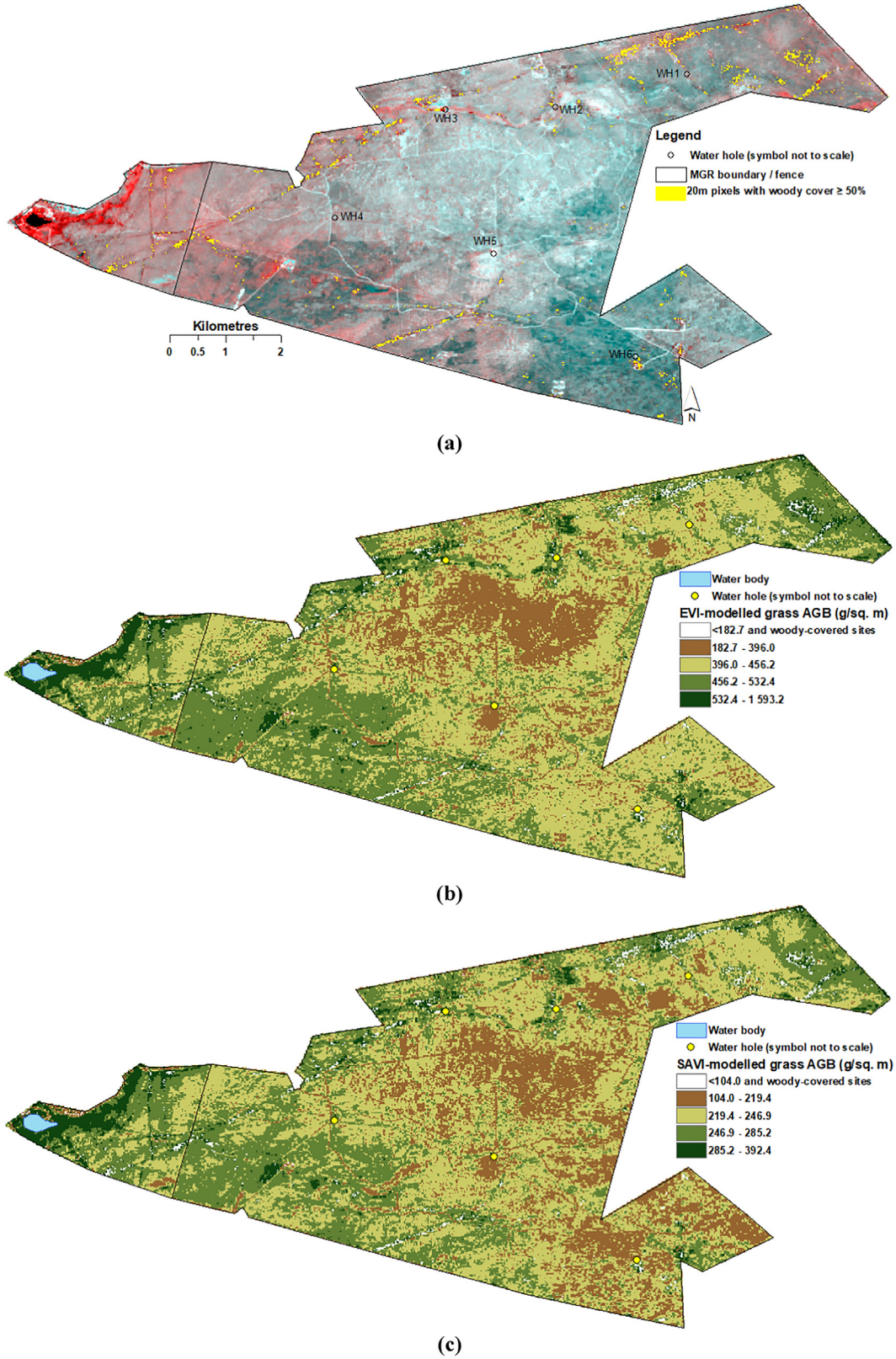

Fig. 7. Rangeland-scale prediction of grass AGB resulting from the application of the models in Fig. 6a and 6b, applied to the woody-masked original (R, G,B = 8a,4,3) Sentinel-2 MSI rainy season (20 March 2020) image (a): the EVI-modelled grass AGB (b), and (c) the SAVI-modelled grass AGB. The EVI had the highest correlation with AGB, followed by the SAVI. Where WH = water hole.

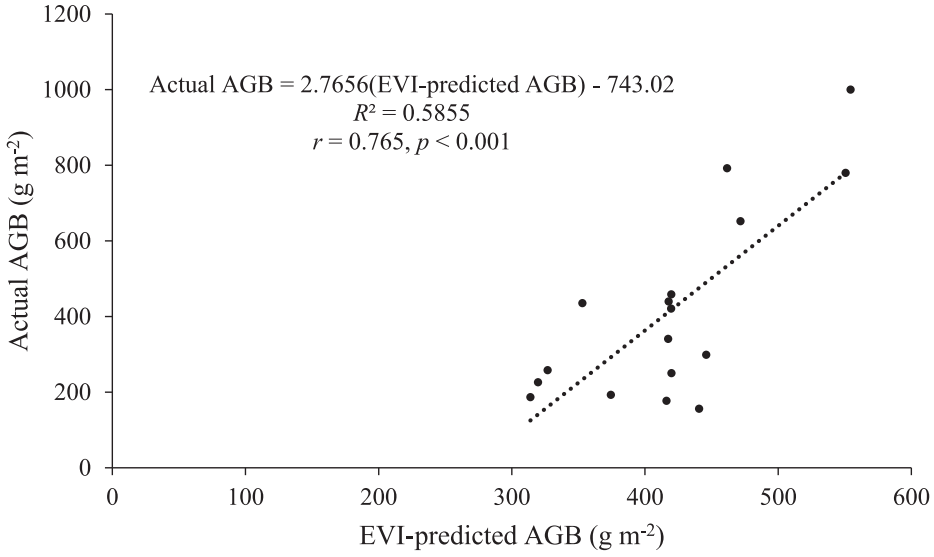

Fig. 8. Predictive relationship between the EVI-modelled AGB values and the actual values from the validation sites.

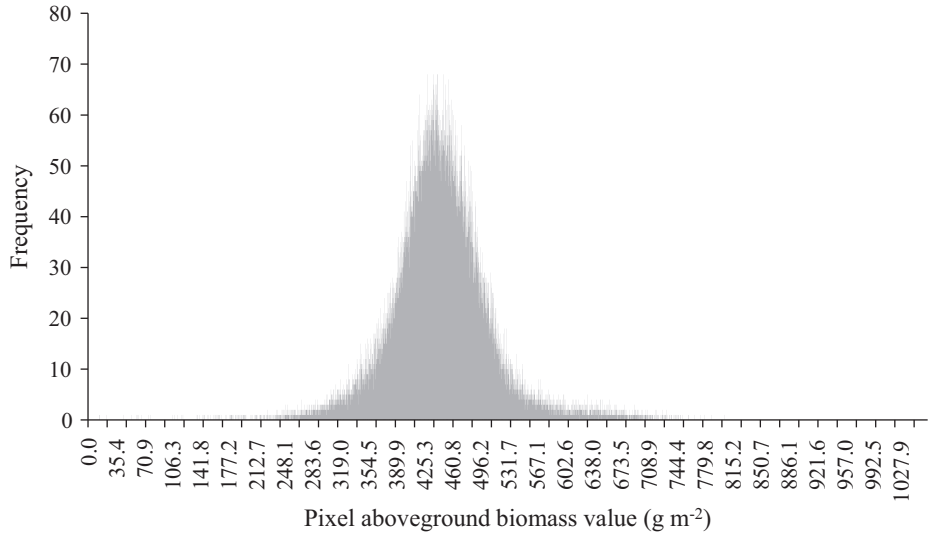

Fig. 9. Frequency distribution of the EVI-modelled grass AGB across the studied rangeland as depicted on the image in Fig. 7a.

cates that most of the rangeland had low biomass. The lowest biomass was from a sampling site near a water hole (WH4, Fig. 7a), where grazing intensity was high. Such highly grazed sites have short grass, which is characteristic of savannah grazing lawns (Hempson et al., 2015).

4.2. Vegetation indices

The results from this study suggest that any of the five VIs that had statistically significant correlations with AGB (EVI, SAVI, NDVI, $AFRI_{2.1\mu m}$, NDWI) can be used to depict spatial variations in grass biomass on savannah rangelands. However, the results suggest that the EVI is the most suitable. Although the correlation coefficients were statistically significant, their values were moderate (Table 4). The physical morphology of the grass species could have caused this. Sampling sites with tall grass species had high field-determined AGB values despite a discontinuous canopy. Dry or senescent leaf and stem tissue at the bases of the grasses, which were tissue remnants from the previous growth season, contributed to the high AGB values. As a consequence, the corresponding VI values at such sites were low, hence the low correlation. Additionally, the grass flowers (illustrated in Fig. 3) tended to have high reflectance in the visible bands, which lowered the values of VIs that employ visible bands (the EVI, NDVI, SAVI; Table 3). Shen et al. (2010) showed that the presence of flowers can result in non-significant correlations between AGB and either NDVI or EVI values.

The EVI-modelled rangeland-scale distribution of AGB in Fig. 7b correctly depicts the *in-situ* AGB due to grazer utilisation. Therefore, the EVI is sensitive to the location

context spatial variations. The heavily-grazed central region of the rangeland, between the water holes, had low AGB on the date of the image. In contrast, the no-grazing section to the west had higher biomass. The statistically significant regression model in Fig. 8 suggests that the rangeland managers can predict AGB at a given site on the rangeland using similar imagery in the future.

The soil-adjusted VIs (EVI, SAVI) performed better than the NDVI. In the savannah rangelands of Etosha National Park, Namibia, Tsalyuk et al. (2017) similarly found that the EVI provided a better model for shrub density ($R^2 = 0.82$) and shrub cover ($R^2 = 0.83$) in comparison with the NDVI on MODIS products. Huete et al. (2002) suggest that the NDVI can perform worse than the EVI since it asymptotically saturates in high biomass scenes, while the EVI remains sensitive to variations in such canopies. This could have been a factor in this study, since the grass was at peak growth and, therefore, some sites had high grass canopy closure. In Fig. 6c, a number of sampling sites that had the highest NDVI had nearly equal values (≈ 0.620) despite large differences in biomass. This is possibly a manifestation of the NDVI's low sensitivity to differences in grass biomass when AGB reaches a critical threshold.

The negative NDWI values for some sampling sites (Fig. 6e) suggest that there was higher SWIR than NIR reflectance at the sites. This could have been caused by sparse grass cover, which permitted high SWIR reflectance from the soil in the grass canopy background (Gao, 1996). Although the red edge indices performed worse than the other VIs, the high correlation coefficient of the REIP indicates the potential usefulness of red edge indices. Forkuor et al. (2020) found that using a Sentinel-2 MSI red edge band (band 6) in a normalised difference vegetation index with the red band (band 4) improved the estimation of aboveground biomass.

Superior performance of the EVI over the NDVI and SAVI has also been observed in temperate grass at peak phenology (Kazar and Warner, 2013). Sparse grass cover could account for the difference between the results in this study and those by Chen et al. (2011b), who found that the NDWI performed better than the NDVI and SAVI in semi-arid rangelands of Idaho, USA. Duan et al. (2012) found that the OSAVI had the best correlation with AGB in relation to grazing intensity in an alpine grassland. On the other hand, Baghi and Oldeland (2019) found that the biomass of the very sparse grass cover on semi-arid, saline grasslands correlated best with the NDVI.

4.3. Potential utility for remotely sensing biomass-related savannah rangeland characteristics

Western et al. (2015) showed that grazing pressure accounted for the fluctuations in savannah pasture biomass quite significantly, in comparison with the influence of drought. Their results underscore the utility of the results in this paper, for monitoring grass AGB *in-situ* in relation to grazing intensity. Since savannahs have the common characteristic of being grass-tree mixtures, the methods that were used in this study are potentially transferable to estimating grass AGB and grazing pressure in other savannah rangelands. The high correlation of the EVI with AGB in another savannah rangeland (Tsalyuk et al., 2017) and in temperate grass (Kazar and Warner, 2013) underscores the transferability potential of the approach that was developed in this study.

Information on the biomass content of a savannah rangeland is important for the estimation of grazer carrying capacity (Palmer et al., 2016). The carrying capacity is usually computed by considering the average body mass of a given grazer species in relation to its dry biomass consumption dietary requirement (Fritz and Duncan, 1994; Dekker, 1997). The approach to estimating grass AGB that is outlined in this study can provide the required data on the amount of grass biomass that is available on the rangeland.

Studies have shown that grass AGB is directly proportional to N and C concentrations in grass (Ullah et al., 2012; Kazar and Warner, 2013; Chapungu et al., 2020). Therefore, the grass AGB quantification method that was used in this study can contribute towards estimating the N and C contents of savannah rangelands. Estimating the C content is useful in studies of rangeland vulnerability to fire, in terms of combustion factors (Hoffa et al., 1999), and fire severity (Smith et al., 2005). Lambin et al. (2003) showed that fires affect savannah areas that have the lowest NDVI and highest surface temperature values. Their results appear to be applicable to senescent grass in the dry season, and suggest that sections of savannah rangelands with high AGB at grass peak growth stage (e.g. the western and south western sections of the study area; Fig. 7b, 7c) have high fire fuel (i.e., high combustion factor). Such sections would, therefore, have more severe fires during the dry season. Mbow et al. (2004) showed that such image-derived indicators of the abundance of fire fuel can be used by rangeland managers to plan the controlled use of fire, as a biomass management tool in conserved savannah areas.

5. Conclusion

A number of vegetation indices that utilise visible, red edge, near infrared, and short wave infrared bands can be used to monitor the grass aboveground biomass of savannah rangelands. They include the EVI, SAVI, NDVI, $AFRI_{2.1\mu m}$, and NDWI. In this study, the EVI was found to be more suitable. Soil-adjusted vegetation indices (EVI, SAVI) performed better than the widely used NDVI in similar studies. The better performance of the EVI is likely to be due to the saturation problem at high biomass, to which the NDVI is vulnerable. The EVI, in comparison, appeared to remain sensitive to biomass variations even at higher AGB levels. The results in this study indicate potential for grazing managers to remotely sense grass AGB and related characteristics of savannah rangelands (e.g. com-

bustion factor, grazer carrying capacity) using the EVI. However, for the grazed savannah rangeland that was studied, the results suggest higher vegetation index prediction accuracy for grazed short-grass biomass than the non-grazed tall grasses. For such tall grass species with high mass per unit area and a discontinuous canopy, vegetation indices can predict low AGB. Given that savannahs have similarities in terms of being characterised by grass and scattered trees, the methods in this study appear to be applicable to estimating aboveground grass biomass in other grazed savannah rangelands.

Declaration of Competing Interest

The authors declare that they have no known competing financial interests or personal relationships that could have appeared to influence the work reported in this paper.

Acknowledgements

This work was funded by a grant from North-West University (NWU), under the Institutional Research Excellence Awards (IREA) scheme. The North West Parks Board authorities are thanked for granting permission for this research and providing transport, personnel (guides, data collection assistants), and accommodation inside Mafikeng Game Reserve during the fieldwork.

References

Barrachina, M., Cristóbal, J., Tulla, A.F., 2015. Estimating above-ground biomass on mountain meadows and pastures through remote sensing. Int. J. Appl. Earth Obs. Geoinf. 38, 184–192.

Baghi, N.G., Oldeland, J., 2019. Do soil-adjusted or standard vegetation indices better predict above ground biomass of semi-arid, saline rangelands in North-East Iran? Int. J. Remote Sens. 40 (22), 8223–8235.

Butterfield, H.S., Malmström, C.M., 2009. The effects of phenology on indirect measures of aboveground biomass in annual grasses. Int. J. Remote Sens. 30 (12), 3133–3146.

Calders, K., Newnham, G., Burt, A., Murphy, S., Raumonen, P., Herold, M., Culvenor, D., Avitabile, V., Disney, M., Armston, J., Kaasalainen, M., 2015. Nondestructive estimates of above-ground biomass using terrestrial laser scanning. Methods Ecol. Evol. 6 (2), 198–208.

Chapungu, L., Nhamo, L., Gatti, R.C., 2020. Estimating biomass of savanna grasslands as a proxy of carbon stock using multispectral remote sensing. Remote Sens. Appl.: Soc. Environ. 17 100275.

Chen, F., Weber, K.T., Anderson, J., Gokhal, B., 2011a. Assessing the susceptibility of semiarid rangelands to wildfires using Terra MODIS and Landsat Thematic Mapper data. Int. J. Wildland Fire 20, 690–701.

Chen, F., Weber, K.T., Gokhale, B., 2011b. Herbaceous biomass estimation from SPOT 5 imagery in semiarid rangelands of Idaho. GIScience & Remote Sensing 48 (2), 195–209.

Clevers, J.G.P.W., De Jong, S.M., Epema, G.F., Van Der Meer, F.D., Bakker, W.H., Skidmore, A.K., Scholte, K.H., 2002. Derivation of the red edge index using the MERIS standard band setting. Int. J. Remote Sens. 23 (16), 3169–3184.

Dekker, B., 1997. Calculating stocking rates for game ranches: Substitution ratios for use in the Mopani Veld. Afr. J. Range Forage Sci. 14 (2), 62–67.

Duan, M., Gao, Q., Wan, Y., Li, Y., Guo, Y., Ganzhu, Z., Liu, Y., Qin, X., 2012. Biomass estimation of alpine grasslands under different grazing intensities using spectral vegetation indices. Canadian J. Remote Sensing 37 (4), 413–421.

Dusseux, P., Hubert-Moy, L., Corpetti, T., Vertès, F., 2015. Evaluation of SPOT imagery for the estimation of grassland biomass. Int. J. Appl. Earth Obs. Geoinf. 38, 72–77.

Eisfelder, C., Kuenzer, C., Dech, S., 2012. Derivation of biomass information for semi-arid areas using remote-sensing data. Int. J. Remote Sens. 33 (9), 2937–2984.

Forkuor, G., Zoungrana, J.B.B., Dimobe, K., Ouattara, B., Vadrevu, K. P., Tondoh, J.E., 2020. Above-ground biomass mapping in West African dryland forest using Sentinel-1 and 2 datasets-A case study. Remote Sens. Environ. 236 111496.

Fritz, H., Duncan, P., 1994. On the carrying capacity for large ungulates of African savanna ecosystems. Proc. Royal Soc. London: Biol. Sci. 256 (1345), 77–82.

Gao, B., 1996. A Normalized Difference Water Index for remote sensing of vegetation liquid water from space. Remote Sens. Environ. 58, 257–266.

Grunow, J.O., 1980. Feed and habitat preferences among some large herbivores on African veld. Proc. Ann. Cong. Grassland Soc. Southern Africa 15 (1), 141–146.

Guerschman, J.P., Hill, M.J., Renzullo, L.J., Barrett, D.J., Marks, A.S., Botha, E.J., 2009. Estimating fractional cover of photosynthetic vegetation, non-photosynthetic vegetation and bare soil in the Australian tropical savanna region upscaling the EO-1 Hyperion and MODIS sensors. Remote Sens. Environ. 113 (5), 928–945.

Hempson, G.P., Archibald, S., Bond, W.J., Ellis, R.P., Grant, C.C., Kruger, F.J., Kruger, L.M., Moxley, C., Owen-Smith, N., Peel, M.J.S., Smit, I.P.J., Vickers, K.J., 2015. Ecology of grazing lawns in Africa. Biol. Rev. 90 (3), 979–994.

Hess, B., Dreber, N., Liu, Y., Wiegand, K., Ludwig, M., Meyer, H., Meyer, K.M., 2020. PioLaG: a piosphere landscape generator for savanna rangeland modelling. Landscape Ecol. 35 (9), 2061–2082.

Hoffa, E.A., Ward, D.E., Hao, W.M., Susott, R.A., Wakimoto, R.H., 1999. Seasonality of carbon emissions from biomass burning in a Zambian savannah. J. Geophys. Res. 104 (D11), 13841–13853.

Huete, A.R., 1988. A soil-adjusted vegetation index (SAVI). Remote Sens. Environ. 25 (3), 295–309.

Huete, A., Didan, K., Miura, T., Rodriguez, E.P., Gao, X., Ferreira, L.G., 2002. Overview of the radiometric and biophysical performance of the MODIS vegetation indices. Remote Sens. Environ. 83 (1), 195–213.

Jucker, T., Caspersen, J., Chave, J., Antin, C., Barbier, N., Bongers, F., Dalponte, M., van Ewijk, K.Y., Forrester, D.I., Haeni, M., et al., 2017. Allometric equations for integrating remote sensing imagery into forest monitoring programmes. Glob. Change Biol. 23 (1), 177–190.

Karnieli, A., Kaufman, Y.J., Remer, L., Wald, A., 2001. AFRI — aerosol free vegetation index. Remote Sens. Environ. 77, 10–21.

Kazar, S.A., Warner, T.A., 2013. Assessment of carbon storage and biomass on minelands reclaimed to grassland environments using Landsat spectral indices. J. Appl. Remote Sens. 7 073583.

Lambin, E.F., Goyvaerts, K., Petit, C., 2003. Remotely-sensed indicators of burning efficiency of savannah and forest fires. Int. J. Remote Sens. 24 (15), 3105–3118.

Louhaichi, M., Hassan, S., Clifton, K., Johnson, D.E., 2018. A reliable and non-destructive method for estimating forage shrub cover and biomass in arid environments using digital vegetation charting technique. Agrofor. Syst. 92 (5), 1341–1352.

Lund, H.G., 2007. Accounting for the world's rangelands. Rangelands 29 (1), 3–10.

Martins, V., Barbosa, C., de Carvalho, L., Jorge, D., Lobo, F., Novo, E., 2017. Assessment of atmospheric correction methods for Sentinel-2 MSI images applied to Amazon floodplain lakes. Remote Sensing 9 (4), 322.

Mbow, C., Goïta, K., Bénié, G.B., 2004. Spectral indices and fire behavior simulation for fire risk assessment in savanna ecosystems. Remote Sens. Environ. 91, 1–13.

Mucina, L., Rutherford, M.C., 2006. Vegetation Map of South Africa, Lesotho and Swaziland: An Illustrated Guide, Strelitzia 19. South African National Biodiversity Institute, Pretoria.

Mundava, C., Schut, A.G., Helmholz, P., Stovold, R., Donald, G., Lamb, D.W., 2015. A novel protocol for assessment of aboveground biomass in rangeland environments. The Rangeland Journal 37 (2), 157–167.
Myint, S.W., 2006. Urban vegetation mapping using sub-pixel analysis and expert system rules: A critical approach. Int. J. Remote Sens. 27 (13), 2645–2665.
Numata, I., Roberts, D.A., Chadwick, O.A., Schimel, J., Sampaio, F.R., Leonidas, F.C., Soares, J.V., 2007. Characterization of pasture biophysical properties and the impact of grazing intensity using remotely sensed data. Remote Sens. Environ. 109, 314–327.
O'Connor, T.G., 1992. Patterns of plant selection by grazing cattle in two savanna grasslands: a plant's eye view. J. Grassland Soc. Southern Africa 9 (3), 97–104.
Palmer, A.R., Samuels, I., Cupido, C., Finca, A., Kangombe, W.F., Yunusa, I.A.M., Vetter, S., Mapaure, I., 2016. Aboveground biomass production of a semi-arid southern African savanna: towards a new model. Afr. J. Range Forage Sci. 33 (1), 43–51.
Peng, Y., Gitelson, A.A., 2012. Remote estimation of gross primary productivity in soybean and maize based on total crop chlorophyll content. Remote Sens. Environ. 117, 440–448.
Porter, T.F., Chen, C., Long, J.A., Lawrence, R.L., Sowell, B.F., 2014. Estimating biomass on CRP pastureland: A comparison of remote sensing techniques. Biomass Bioenergy 66, 268–274.
Price, B., McAlpine, C.A., Kutt, A.S., Phinn, S.R., Pullar, D.V., Ludwig, J.A., 2009. Continuum or discrete patch landscape models for savanna birds? Towards a pluralistic approach. *Ecography* 32 (5), 745–756.
Qi, J., Chehbouni, A., Huete, A.R., Kerr, Y.H., Sorooshian, S., 1994. A modified soil adjusted vegetation index. Remote Sens. Environ. 48 (2), 119–126.
Quan, X., He, B., Yebra, M., Yin, C., Liao, Z., Zhang, X., Li, X., 2017. A radiative transfer model-based method for the estimation of grassland aboveground biomass. Int. J. Appl. Earth Obs. Geoinf. 54, 159–168.
Rondeaux, G., Steven, M., Baret, F., 1996. Optimization of soil adjusted vegetation indices. Remote Sens. Environ. 55 (2), 95–107.
Rouse, J.W., Haas, R.H., Schell, J.A., Deering, D.W., 1974. Monitoring vegetation systems in the Great Plains with ERTS. In: NASA, Third ERTS Symposium. NASA, Washington, DC, pp. 309–317.
Samimi, C., Kraus, T., 2004. Biomass estimation using Landsat-TM and-ETM+. Towards a regional model for Southern Africa? GeoJournal 59 (3), 177–187.
Scheiter, S., Schulte, J., Pfeiffer, M., Martens, C., Erasmus, B.F., Twine, W.C., 2019. How does climate change influence the economic value of ecosystem services in savanna rangelands? Ecol. Econ. 157, 342–356.
Schino, G., Borfecchia, F., De Cecco, L., Dibari, C., Iannetta, M., Martini, S., Pedrotti, F., 2003. Satellite estimate of grass biomass in a mountainous range in central Italy. Agrofor. Syst. 59, 157–162.
Shen, M., Chen, J., Zhu, X., Tang, Y., Chen, X., 2010. Do flowers affect biomass estimate accuracy from NDVI and EVI? Int. J. Remote Sens. 31 (8), 2139–2149.
Smith, A.M.S., Wooster, M.J., Drake, N.A., Dipotso, F.M., Falkowski, M.J., Hudak, A.T., 2005. Testing the potential of multi-spectral remote sensing for retrospectively estimating fire severity in African savannahs. Remote Sens. Environ. 97, 92–115.
Tsalyuk, M., Kelly, M., Getz, W.M., 2017. Improving the prediction of African savanna vegetation variables using time series of MODIS products. ISPRS J. Photogramm. Remote Sens. 131, 77–91.
Ullah, S., Si, Y., Schlerf, M., Skidmore, A.K., Shafique, M., Iqbale, I.A., 2012. Estimation of grassland biomass and nitrogen using MERIS data. Int. J. Appl. Earth Obs. Geoinf. 19, 196–204.
Western, D., Mose, V.N., Worden, J., Maitumo, D., 2015. Predicting extreme droughts in savannah Africa: A comparison of proxy and direct measures in detecting biomass fluctuations, trends and their causes. PLoS ONE 10 (8).
Zumo, I.M., Hashim, M., Hassan, N., 2021. Mapping grass above-ground biomass of grazing-lands using satellite remote sensing. Geocarto Int., 1–14